Robust turbulence modelling of complex wall-bounded flows with heat transfer

M. POPOVAC and K. HANJALIĆ
Department of Multi-scale Physics
Faculty of Applied Sciences
Delft University of Technology
Lorentzweg 1, 2628 CJ Delft
THE NETHERLANDS
http://www.ws.tn.tudelft.nl

Abstract: In order to make Durbin's $\overline{v^2}$-f model robust and applicable for calculation of complex turbulent flows with heat transfer, we proposed replacement of variables so that the transport equation for $\zeta = \overline{v^2}/k$ is solved instead of $\overline{v^2}$. Scrutinising and extending the work of Kader, we are presenting compound wall treatment which defines appropriate boundary condition for the flow quantities, according to the given mesh and local flow conditions, regardless of the position of the near-wall cell. It combines the integration up to the wall and the wall function approach using physical rationale which are described. This wall treatment is general approach for near-wall region turbulence modelling, but here it is presented in conjunction with ζ-f model. The computations of standard generic test cases (steady and pulsating channel, backward-facing, wavy hillstep and round impinging jet) using proposed near-wall treatment give satisfactory agreement of the results with experiments and DNS data.

Keywords: RANS, wall functions, compound wall treatment, elliptic relaxation, ζ-f, $\overline{v^2}$-f

1 Introduction

Capturing and resolving near-wall effects is crutial for accurate prediction of wall bounded turbulent flow characteristics. In that sense the elliptic relaxation model of Durbin [1] brings significant improvement, in comparison to standard k-ε, by introducing the transport equation for wall-normal Reynolds stress component $\overline{v^2}$ (which describes better the Reynolds stress anisotropy) and elliptic relaxation function f (which captures non-viscous wall effects).

However, despite the fact that $\overline{v^2}$-f model is giving much better results then k-ε model for many complex turbulent flows with heat transfer, it is still not widely used for engineering purposes because of its restrictions: near-wall behaviour, boundary condition for f and mesh quality near the wall.

In order to overcome these shortcomings, we proposed a modification of Durbin's eddy-viscosity model in which the transport equation for the velocity scale ratio $\zeta = \overline{v^2}/k$ is solved, instead of the equation for $\overline{v^2}$ [11]. The reason for this development originated from the desire to improve the numerical stability of the model, especially when using segregated solvers.

Another novelty that we proposed is the application of a quasi-linear pressure-strain model in equation for f, based on the formulation of Speziale, Sarkar and Gatski [3], instead of using basic IP model. This brings some improvement especially for the non-equilibrium wall flows.

In order to ease the mesh quality requirements we proposed the wall treatment which reduces either to standard integration to the wall (when a near-wall cell is in the viscous sublayer) or to appropriate wall functions approach (when a near-wall cell lays in a fully turbulent layer) according to the given mesh and local flow conditions [18]. This wall treatment combines the wall limiting value and the farfield value of given variable through the unified expression suggested by Kader [2], making redundant in that way the information about the size or the distribution of the near-wall cells.

The computations of flow and heat transfer in a plane channel, behind a backward fac-

ing step and in a round impinging jet show in all cases satisfactory agreement with experiments and direct numerical simulations.

2 The ζ-f model

The modification of original Durbin's model [1] is done by introducing normalised velocity scale $\zeta = \overline{v^2}/k$, which represents the ratio of the two time scales: k/ε and $\overline{v^2}/\varepsilon$. The transport equation for ζ, which can easily be derived from the transport equations for $\overline{v^2}$ and k, is solved instead of the transport equation for $\overline{v^2}$. The direct transformation yields:

$$\frac{D\zeta}{Dt} = f - \frac{\zeta}{k}\mathcal{P} + \frac{\partial}{\partial x_k}\left[\left(\nu + \frac{\nu_t}{\sigma_\zeta}\right)\frac{\partial \zeta}{\partial x_k}\right] + X \tag{1}$$

where $X = \frac{2}{k}\left(\nu + \frac{\nu_t}{\sigma_\zeta}\right)\frac{\partial \zeta}{\partial x_k}\frac{\partial k}{\partial x_k}$ is "cross diffusion" which comes as a consequence of the transformation.

The form of the equation with the cross diffusion X retained represents pure transformation of transport equation for $\overline{v^2}$ into ζ equation. Although X has certain influence close to the wall, it can be omitted in order to retain a simple source-sink-diffusion form of the transport equation, and the omission can be compensated by re-tuning some of the coefficients. In case of retaining the original form of the transport equation (X included) no modification of model coefficients is needed. But apart from an extra implementation effort, the intervention on X is needed in this case: k, which is in the denominator of X, goes to zero close to the wall, and therefore it has to be limited similarly to the time scale limiting with its Kolmogorov value.

Even though by solving either ζ or $\overline{v^2}$ equation one should get the same result, there is improved numerical stability when ζ approach is used in comparison to its $\overline{v^2}$ counterpart. In that sense following advantages from the computational point of view can be identified:

- instead of ε appearing in the $\overline{v^2}$ equation, which has a non-zero value at the wall that is difficult to reproduce correctly in the near-wall layer, the ζ equation contains the turbulence kinetic energy production $\mathcal{P}$, which has zero value at the wall and is much easier to reproduce accurately if the local turbulent stress and the mean velocity gradient are captured properly.

- in $\overline{v^2}$ equation three terms on the right hand side have to be in balance very close to the wall since all three are proportional to y^2, whereas in ζ equation only f and $\mathcal{D}\zeta$ have to be in balance very close to the wall, since $\mathcal{P}\zeta/k$ goes to zero faster then other two. This is important especially when segregated solvers are used.

- the boundary condition for f deduced from the budged of ζ equation in the limit when the wall is approached reads:

$$f_w = \lim_{y\to 0}\frac{-2\nu\zeta}{y^2} \tag{2}$$

  i.e. there is in the denominator the minimal distance to the wall to the power two (y^2), and not to the power four (y^4) like in the $\overline{v^2}$-f model. This boundary condition is certainly less stiff which contributes to improved robustness, but also it is of the same form as ε_w and therefore it can be treated in analogous manner in the computational procedure.

This simple transformation from $\overline{v^2}$ to ζ introduces another perspective in understanding the turbulent quantities. Being normalised and dimensionless, ζ is appropriate measure of the flow anisotropy, better then $\overline{v^2}$ alone, because it describes the flow anisotropy in respect to local flow conditions. In that sense one can mathematically derive the limiting values for ζ, using Schwarz inequality $\overline{u_i u_i} > 0$ and the definition of turbulent kinetic energy $k = \overline{u_l u_l}/2$, whereas for $\overline{v^2}$ no such a constrain can be defined.

$$\frac{\overline{uu}}{k} + \frac{\overline{vv}}{k} + \frac{\overline{ww}}{k} = 2$$

$$\text{for} \quad \frac{\overline{uu}}{k} \to 0 \quad \text{and} \quad \frac{\overline{ww}}{k} \to 0 \tag{3}$$

$$0 \le \frac{\overline{vv}}{k} = \zeta \le 2$$

and in case of isotropic flow conditions, $\overline{uu} = \overline{vv} = \overline{ww}$ the value of ζ is:

$$3\left(\frac{\overline{vv}}{k}\right)_i = 2 \qquad (4)$$
$$\zeta_i = 2/3$$

so from the value of ζ one can immediately see how much and in which direction (reducing wall-normal Reynolds stress component when ζ is close to zero, or reducing other two normal components of Reynolds stress tensor if ζ is close to two) is certain flow region departing from the isotropic flow conditions.

Note that physically the constrain from Eq. (3) is even tougher because the equality is valid only when the Reynolds stress normal components involved are equal to zero, which cannot occur in reality.

2.1 Quasi-linear pressure strain term

Instead of using linear IP model for the rapid part of the pressure strain term, which is a standard practice used in $\overline{v^2}$-f model, we adopted more advanced quasi-linear model of Speziale *et al.* (SSG) [3]:

$$\begin{aligned}\Pi_{ij,2} = \; & -C_2'\mathcal{P}a_{ij} + C_3 k S_{ij} \\ + \; & C_4 k(a_{ik}S_{jk} + a_{jk}S_{ik} - \tfrac{2}{3}\delta_{ij}a_{kl}S_{kl}) \\ + \; & C_5 k(a_{ik}\Omega_{jk} + a_{jk}\Omega_{ik})\end{aligned} \qquad (5)$$

which was found to capture better the stress anisotropy in the wall boundary layers.

Applying this model to the wall normal stress component $\Pi_{22,2}$ and using standard assumption $\mathcal{P}_{22} = 0$, the following form of the f equation in conjunction with the ζ equation with $X = 0$ is obtained:

$$\begin{aligned}L^2\nabla^2 f - f = \; & \tfrac{1}{\tau}\left(c_1 + C_2'\tfrac{\mathcal{P}}{\varepsilon}\right)\left(\zeta - \tfrac{2}{3}\right) \\ - \; & \left(\tfrac{C_4}{3} - C_5\right)\tfrac{\mathcal{P}}{k}\end{aligned} \qquad (6)$$

Adopting the coefficients for the SSG pressure-strain model, with $C_4 = 0.625$ and $C_5 = 0.2$, and noting that the last term in Eq. (6) can be neglected because $(C_4/3 - C_5) \approx 0.008$ as compared with the first term, we arrive to the following set of model equations constituting the ζ-f model:

$$\nu_t = C_\mu^D \zeta k \tau \qquad (7)$$

$$\frac{Dk}{Dt} = \mathcal{P} - \varepsilon + \frac{\partial}{\partial x_j}\left[(\nu + \frac{\nu_t}{\sigma_k})\frac{\partial k}{\partial x_j}\right] \qquad (8)$$

$$\frac{D\varepsilon}{Dt} = \frac{(C_{\varepsilon 1}\mathcal{P} - C_{\varepsilon 2}\varepsilon)}{\tau} + \frac{\partial}{\partial x_j}\left[(\nu + \frac{\nu_t}{\sigma_\varepsilon})\frac{\partial \varepsilon}{\partial x_j}\right] \qquad (9)$$

$$L^2\nabla^2 f - f = \frac{1}{\tau}\left(C_1 - 1 + C_2'\frac{\mathcal{P}}{\varepsilon}\right)\left(\zeta - \frac{2}{3}\right) \qquad (10)$$

$$\frac{D\zeta}{Dt} = f - \frac{\zeta}{k}\mathcal{P} + \frac{\partial}{\partial x_k}\left[\left(\nu + \frac{\nu_t}{\sigma_\zeta}\right)\frac{\partial \zeta}{\partial x_k}\right] \qquad (11)$$

with the time and length scale limited with the Kolmogorov values as the lower bounds, and Durbin's realisability constraints [13] as the upper bounds:

$$\tau = max\left[min\left(\tfrac{k}{\varepsilon}, \tfrac{a}{\sqrt{6}C_\mu^D|S|\zeta}\right) C_\tau \left(\tfrac{\nu^3}{\varepsilon}\right)^{1/2}\right] \qquad (12)$$

$$L = C_L\, max\left[min\left(\tfrac{k^{3/2}}{\varepsilon}, \tfrac{k^{1/2}}{\sqrt{6}C_\mu^D|S|\zeta}\right) C_\eta \left(\tfrac{\nu^3}{\varepsilon}\right)^{1/4}\right] \qquad (13)$$

where the coefficient a takes its recommended value $a = 0.6$.

A special attention is needed to the implementation of the realisability constraints. Some authors are imposing the time and length scale obtained from the realisability considerations simply as an upper bound to previously defined time and length scale (higher value between Kolmogorov and large eddy scale). However, that can lead to unphysical situation (e.g. in the initial phase of the computation, or in the farfield of the stagnation region) that the computed time or length scale gets smaller than the Kolmogorov scale. For example at the beginning of the computation, if the flow field is not initialised properly, the realisability time or length scale can get the value almost zero, whereas the Kolmogorov definition would certainly give the value higher than that. Therefore one

has to be carefull: Durbin's realisability constraints can be used only as the upper bounds to the large eddy scales, whereas the Kolmogorov scales remain the smallest scales of eddies in the flow.

2.2 The model coefficients

It was mentioned earlier that because of the omission of X, some of the coefficients needed to be re-tuned. The most important change is the one for the length scale coefficient, because L influences the value of f, and f is the only term which can compensate the omitted term in the ζ equation. It has been chosen to increase the value of C_L so that the level of L is increased throughout the domain, and not just the Kolmogorov length scale (that would be achieved by increasing C_η) which is valid only close to the wall. This is because otherwise the influence of viscous effects would be extended further into the fully turbulent region, even if with original coefficients Kolmogorov length scale is already active far beyond the viscous sublayer for which it was derived. The agreement with DNS results gave the value of 0.36 for C_L instead of its standard value 0.22

The other three coefficients which are changed ($C_{\varepsilon 1}$, σ_ζ and C_2') are slightly modified, still according to their constrains, for a fine tuning reasons. In the definition of $C_{\varepsilon 1}$ the square root was dropped, and subsequently the coefficients in front of the square root changed to 0.012, in order to make it more sensitive for establishing the recovery region. The value for σ_ζ was changed from 1.0 to 1.2 in order to get better agreement with DNS results, especially in the wake region. As for the C_2', its original SSG value has been reduced by about 20% on the same ground as Durbin reduced the original LRR value of c_1 in same proportion in order to take into account the discrepancy in the definition of ε in the log-law region.

The final set of model coefficient which are used (note the reformulation of $C_{\varepsilon 1}$) is given in Table. (1).

3 Simplified analytical wall function

If RANS equations are solved all the way to the wall, then the model which is used has to include the near-wall effects: non-viscous wall-blocking and viscous damping. In this case exact boundary conditions for flow variables can be imposed on the solid boundary, and the accuracy of the flow calculations in reproducing local non-equilibrium flow effects (separation, impingement etc.) depends on how accurate these effects are described by the model. The price one has to pay for this approach is a very fine mesh resolution near the wall, which can be a limiting factor in case of complex flow calculations.

However, when the coarse mesh is used so that the first near-wall cell is in the fully turbulent region, the majority of the local near-wall effects are not resolved. In this case the wall functions, which relate the values of the variables in the cell centres with those at the wall through pre-integrated simplified expressions, are used to define the boundary conditions at the wall. But simplifications used for deriving standard wall functions do not include any non-equilibrium effects, like e.g. in the log-law which reads:

$$U^+ = \frac{1}{\kappa} \ln \left(E y^+ \right) \tag{14}$$

where $\kappa = 0.41$ is Von Karman's constant, $E = 8.34$ is the log-law additive constant, and $y^+ = u_\tau y/\nu$ is normalised distance from the wall.

Standard log-law is obviously correct only for the equilibrium flow conditions, so in order to recover at least a part of non-equilibrium effects the wall function expression has to include the non-equilibrium terms. Following the argumentation of Craft *et al.* [12] the momentum equation is analytically integrated for the near-wall cell, including thus the convection and the pressure gradient, abandoning all traditional assumptions and using only one: the distribution of the viscosity profile in the near-wall region. Simplification being made is that close to the wall the flow is considered to be two-dimensional, so the momentum equation reads:

C_μ^D	$C_{\varepsilon 1}$	$C_{\varepsilon 2}$	c_1	C_2'	σ_k	σ_ε	σ_ζ	C_τ	C_L	C_η
0.22	$1.4(1+0.012/\zeta)$	1.9	0.4	0.65	1	1.3	1.2	6.0	0.36	85

Table 1: Coefficients used for ζ-f model

$$\rho\frac{\partial U}{\partial t}+\rho U\frac{\partial U}{\partial x}+\rho V\frac{\partial U}{\partial y}=\frac{\partial}{\partial y}\left[(\mu+\mu_t)\frac{\partial U}{\partial y}\right]-\frac{\partial p}{\partial x} \tag{15}$$

where t is the time, U and V are the velocity vector components in the wall-tangential and wall-normal direction respectively (denoted as x and y coordinates, as shown on Fig. 1), p is the pressure, and μ and μ_t are dynamic molecular and turbulent viscosity respectively.

The approximation of time variation $\partial U/\partial t$, the convection $U_i\partial U/\partial x_i$ and the pressure gradient along the direction tangential to the wall $\partial p/\partial x$ is that they are considered to be constant across the near-wall cell, and known from the previous time step or previous iteration. For simplicity these three terms together will be denoted as C_{tan}:

$$C_{tan}=\rho\frac{\partial U}{\partial t}+\rho U\frac{\partial U}{\partial x}+\rho V\frac{\partial U}{\partial y}+\frac{\partial p}{\partial x} \tag{16}$$

The most common assumption for the variation of the turbulent viscosity throughout the near-wall cell is to divide it into two regions (see Fig. 1): viscous sublayer where turbulent viscosity equals zero (only the molecular viscosity plays role there), and fully turbulent region where due to the mixing length theory a linear variation is assumed:

$$\mu_t=\begin{cases}0 & \text{for } y<y_v\\ \\ \rho\kappa u_\tau y & \text{for } y\geq y_v\end{cases} \tag{17}$$

where y_v is the thickness of the viscous sublayer which is defined from the experiments.

There are a few definitions of characteristic friction velocity u_τ, traditional one being $u_\tau=\sqrt{\tau_w/\rho}$. But here we will adopt the friction velocity defined through the turbulent kinetic energy:

$$u_\tau=c_\mu^{1/4}k^{1/2} \tag{18}$$

where $c_\mu=0.09$.

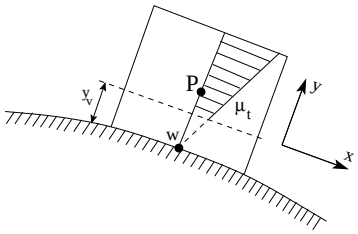

Figure 1: Sketch of the near-wall cell with the assumed turbulent viscosity

Following the expression (17), the simplified momentum equation (15) is integrated over two distinct regions. Boundary conditions used to determine the constants of these two integrations are the continuity and the smoothness of the velocity profile at the interface y_v, and its known values at the wall $U_w=0$ and in the cell centre $U_p=U_{tan}$. After the integration following expression for the wall shear stress is obtained:

$$\tau_w=\frac{U-\dfrac{C_{tan}y}{\kappa u_\tau}}{\dfrac{y_v}{\mu}+\dfrac{\ln\left(\dfrac{y}{y_v}\right)}{\kappa u_\tau}} \tag{19}$$

which is used when the near-wall cell is in the fully turbulent region.

In order to compare with Eq. (14), we will rearrange Eq. (19) to get the form recognisable from standard log-law. We can rewrite the denominator of Eq. (19) as follows:

$$\frac{y_v}{\mu}+\frac{\ln\left(\dfrac{y}{y_v}\right)}{\kappa u_\tau}=\frac{1}{\kappa u_\tau}\left[\frac{\kappa u_\tau y_v}{\mu}+\ln\left(\frac{y}{y_v}\right)\right]=$$

$$=\frac{1}{\kappa u_\tau}\ln\left(\frac{e^{\kappa y_v^+}y^+}{y_v^+}\right)=\frac{1}{\kappa u_\tau}\ln\left(Ey^+\right)$$

$$y^+=\frac{u_\tau y}{\nu} \tag{20}$$

because inserting the standard value for the viscous sublayer thickness $y_v^+=11$ one gets

$e^{\kappa y_v^+}/y_v^+ = 8.3$, which is the value of the additive constant in the standard log-law. This gives the physical meaning of the constant E.

In the nominator of Eq. (19) we will extract the velocity, and treat jointly all the other terms:

$$U - \frac{C_{tan} y}{\kappa u_\tau} = U\left(1 - \frac{C_{tan} y}{U \kappa u_\tau}\right) = U\psi$$
$$\psi = 1 - \frac{C_{tan} y}{U \kappa u_\tau} \tag{21}$$

where ψ is introduced for simplicity, in terms of normalised values it reads:

$$\psi = 1 - \frac{C_{tan}^+ y^+}{U^+ \kappa}$$
$$C_{tan}^+ = \frac{\nu}{{u_\tau}^3}\left[\rho\frac{\partial U}{\partial t} + \rho U\frac{\partial U}{\partial x} + \rho V\frac{\partial U}{\partial y} + \frac{\partial p}{\partial x}\right] \tag{22}$$

and it defines the importance of the non-equilibrium terms relative to its equilibrium counterpart.

Finally, inserting Eq. (20) and Eq. (21) into Eq. (19) the simplified analytical wall function in normalised form is obtained:

$$U^+ = \frac{1}{\kappa\psi}\ln\left(Ey^+\right) \tag{23}$$

which resembles standard log-law (Eq. 14), but with the correction factor ψ included which accounts for local non-equilibrium flow effects. Naturally, for the equilibrium flow conditions ($C_{tan} = 0$, thus $\psi = 1$) Eq. (23) reduces to standard log-law (Eq. 14).

The difference between the work of Craft *et al.* and this simplified analytical wall function is that we slightly modified the turbulent viscosity profile. In order to have a continuous turbulent viscosity distribution they adopted the profile which is shifted from the wall for y_v, i.e. $\mu_t = \rho\kappa u_\tau(y - y_v)$. But to compensate this shifting they defined the viscous subleter thickness $y_v^+ = 5.9$, which is almost half of the one we adopted. Their assumption, however, leads to cumbersome wall function expressions, so we used Eq. (17) which gives simplier expressions without any significant change in its performance.

4 Compound wall treatment

So far we were considering two separate near-wall modelling cases in respect to the definition of the boundary conditions: turbulence models with the integration to the wall (when exact boundary conditions are imposed at the wall), and models with the wall function approach (when the boundary conditions are defined from the wall function expressions). In order to use either integration to the wall or the wall function approach, the near-wall cell has to ley in the viscous sublayer or a fully turbulent region respectively.

But it is difficult to assure, especially in case of complex flows, that all near-wall cells (or great majority of them) ley in one or another region. And since these two approaches cannot be used together, because of their mesh requirements which are excluding each other, there is a need for a unified method in defining the boundary conditions. Based on Kader's idea, we proposed the *compound wall treatment* (CWT) [18].

The starting point for such a wall treatment are the two limiting boundary condition definitions, the viscous and the fully turbulent, so the problem that remains is how to combine the two to get the correct behaviour throughout the near-wall region. In order to analyse the possibilities for doing this, we will consider the wall shear stress. The viscous and the fully turbulent definitions of τ_w are:

$$\tau_w^v = \nu\frac{U_p}{y_p}$$
$$\tau_w^t = \frac{u_\tau}{\kappa\psi}\ln\left(Ey^+\right) \tag{24}$$

where subscripts "p" and "w" denote the values of the variables in the cell centre and at the wall respectively (see Fig. 1).

In case of the plane channel flow (DNS $Re_\tau = 800$, [5]) the definitions given by Eq. (24) are presented on Fig. (2). One can see that the viscous definition reproduces the exact boundary value at the wall, it fits the DNS profile in the viscous sublayer (approximately $y^+ < 5$) and drops to zero further away. The fully turbulent definition goes from zero at the wall to exact value in the fully turbulent region (approximately $y^+ > 30$). In

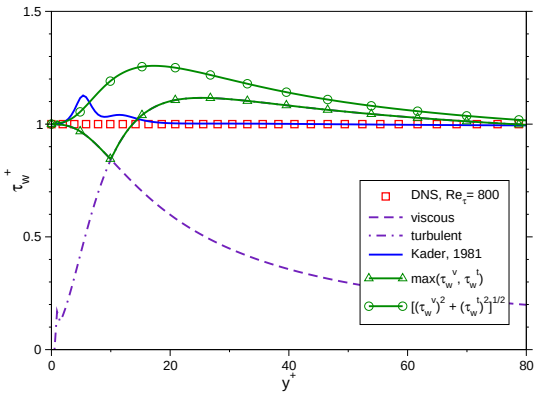

Figure 2: The viscous and the fully turbulent definitions of τ_w (Eq. 24), and *a-priori* evaluation of the considered blending models (equations 25, 26 and 32). Symbols: DNS of Tanahashi *et al.* [5].

the buffer region ($5 < y^+ < 30$) both definitions give approximately the same values.

An easy choice for combining the two limiting values is to take their quadratic mean, as proposed by Esch and Menter [4]:

$$\phi_p = \sqrt{\phi_v^2 + \phi_t^2} \tag{25}$$

where ϕ is the considered variable, the subscript "v" denotes the viscous value, and "t" the fully turbulent value of that variable.

As shown on Fig. (2), the expression (25) does have the correct limiting behaviour: it is reducing to the viscous or the fully turbulent value in their respective regions. But the overestimation produced by Eq.(25) in the buffer region indicates that there is no physical background for such a wall treatment – it simply represents the mathematical connecting of the two values. One can also generalise the expression (25) by using $(\phi_v^n + \phi_t^n)^{1/n}$ to obtain better approximation in the buffer layer, but the author's experience with $n = 4$ produced only marginal improvement.

In the buffer region both the viscous and the turbulent effects are of the same importance, and both viscous and the fully turbulent definitions of boundary conditions give approximately the same value. Therefore either of the two definitions alone is better approximation than their quadratic mean. Furthermore note that one definition gives correct value in the region where the other gives much lower one (see Fig. 2). This means that a simple switching formula can also be used as the near wall treatment (especially for the variables like ε, which have a strong variation in the wall region):

$$\phi_p = max\left(\phi_v, \phi_t\right) \tag{26}$$

and its *a-priori* evaluation in case of τ_w for the plane channel flow is also shown in Fig. (2).

But just like Eq. (25), the relation (26) does not give a satisfactory result in the buffer region, since there is no physical justification for this switching. In order to have correct behaviour in the buffer region one has to combine the viscous and fully turbulent values with some physical sound, i.e. the transition in the treatment of the two regions has to be done through some flow quantity.

We considered the blending of the wall-limiting and fully turbulent properties based on the idea of Kader [2], who proposed unique temperature profile throughout the whole wall boundary layer:

$$\Theta^+ = Pry^+ e^{-\Gamma_\Theta} + \left[\alpha \ln\left(y^+\right) + \beta\left(Pr\right)\right] e^{-1/\Gamma_\Theta} \tag{27}$$

where $\Theta^+ = (T_w - T)\rho c_p u_\tau / q_w$ is the normalised temperature difference, $\alpha = 2.12$ and $\beta(Pr) = (3.85Pr^{1/3} - 1.3)^2 + 2.12\ln(Pr)$ are thermal boundary layer constants, and the exponent of the blending function Γ_Θ is a function of the normalised distance to the wall $y^+ = u_\tau y/\nu$:

$$\Gamma_\Theta = \frac{0.01\left(Pry^+\right)^4}{1 + 5Pr^3 y^+} \tag{28}$$

Putting $Pr = 1$ in Eq. (27), with standard values for log-law constants adopted (Eq. 14), we are obtaining analogous expression for the mean velocity:

$$U^+ = y^+ e^{-\Gamma} + \left[\frac{1}{\kappa}\ln\left(Ey^+\right)\right] e^{-1/\Gamma} \tag{29}$$

and by putting $Pr = 1$ into Eq. (28) the exponent of the blending function becomes:

$$\Gamma = \frac{0.01 y^{+4}}{1 + 5y^+} \tag{30}$$

where all these terms are shown on Fig. (3) in case of the plane channel flow (DNS $Re_\tau = 800$, [5]).

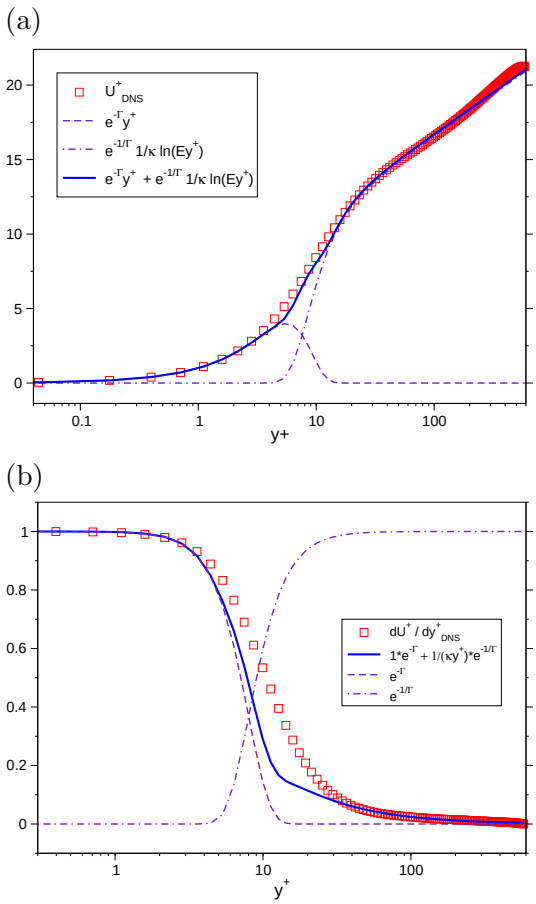

Figure 3: Terms in Kader's expression: blended velocity profile (a), velocity derivative and blending functions (b).

Expressions (27) and (29) define the blending of the viscous and the fully turbulent definition of Θ^+ and U^+ respectively. Although Kader [2] offered no physical justification for these expressions, one can argue that the blending functions $e^{-\Gamma\Theta}$ and $e^{-\Gamma}$ represent the solution of a simplified 1-D elliptic blending equation:

$$\alpha(y) - \ell^2 \frac{d^2\alpha(y)}{dy^2} = 1$$
$$\alpha(y) = 1 - e^{-y/\ell} \qquad (31)$$
$$\phi = \phi_v(1-\alpha) + \phi_t\alpha$$

where the characteristic length scale ℓ is assumed to be constant, the boundary conditions used $\alpha \to 0$ for $y \to 0$ and $\alpha \to 1$ for $y \to \infty$, and the variables replaced $e^{-\Gamma} = 1 - \alpha$.

In Eq. (29), however, the blending function of the fully turbulent part ϕ_t was replaced with $e^{-1/\Gamma}$ instead of $(1 - e^{\Gamma})$. This does not have to be wrong, because due to uncertainty of both viscous and fully turbulent definition of the boundary condition in the buffer region one cannot require the sum of the blending functions to give unity. In addition, the exponent in Eq. (30) was set to be proportional to $-y^3$, unlike Eq. (31) where it is proportional to $-y$. However, similar idea is pursued also for the elliptic blending turbulence models, where the blending formula is used in the form: $\phi = \phi_v(1-\alpha^2) + \phi_t\alpha^2$.

Despite these two small differences, the principle of the elliptic blending is obvious in Kader's expression (Eq. 29). So now we expand this principle to other properties for which continuous boundary conditions are required (in ζ-f model those are $\mathcal{P}$ and ε, whereas for f a specific near-wall treatment is used):

$$\phi = \phi_v e^{-\Gamma} + \phi_t e^{-1/\Gamma} \qquad (32)$$

and its behaviour in case of τ_w^+ for the channel flow (DNS $Re_\tau = 800$, [5]) was already shown on Fig. (2). One can clearly see that apart from a small deviation for y^+ between 5 and 10 due to a minor deficiency in Eq. (29) (see Fig. 3), the resulting τ_w^+ is in very good agreement with the DNS data and superior to expressions (25) and (26).

4.1 Kinetic energy production

The flow calculations with sufficiently fine mesh resolution in the near-wall region will reproduce correctly both the turbulent stress and the velocity gradient. This gives a correct profile of $\mathcal{P}$, as represented for the plane channel flow (DNS $Re_\tau = 800$, [5]) on Fig. (4a) with dashed lines. When the coarse mesh is used, however, neither the turbulent stress nor the velocity gradient can be obtained correctly. Therefore in standard wall function approach the value of $\mathcal{P}$ is imposed assuming local equilibrium conditions: logarithmic velocity profile and constant shear stress. This gives a simple relation $\mathcal{P} = {u_\tau}^3/(\kappa y)$ (dash-dotted lines on Fig. 4a), but it is correct only

in the fully turbulent region in equilibrium flows.

However, once we have the analytical expression for the velocity distribution across the near-wall region, we can derive an expression for $\mathcal{P}$ by taking $(\partial U/\partial y)$ obtained from Eq. (29) (see Fig. 3) in combination with the near-wall and fully turbulent expressions for the turbulent stress. This, basically, reduces to the blending according to Eq. (32), where ϕ_v here is the fine resolution $\mathcal{P}$ value from integration to the wall, and ϕ_t is the coarse mesh wall function $\mathcal{P}$ values:

$$\mathcal{P}_p = -\overline{uv}\frac{\partial U}{\partial y} = C_\mu \zeta_p \frac{k_p^2}{\varepsilon_p}\left(\frac{\partial U}{\partial y}\right)_p^2 e^{-\Gamma} + \frac{c_\mu^{3/4} k_p^{3/2}}{\psi_p \kappa y_p} e^{-1/\Gamma} \tag{33}$$

Note that here $C_\mu = 0.22$ and $c_\mu = 0.07$. Figure (4a) shows $\mathcal{P}$ from Eq. (33), compared with the integration to the wall and the wall function approaches.

4.2 Energy dissipation rate

The viscous and the fully turbulent definition of the turbulence kinetic energy dissipation rate are:

$$\varepsilon_v = \frac{2\nu k_p}{y_p^2}, \qquad \varepsilon_t = \frac{c_\mu^{3/4} k_p^{3/2}}{\kappa y_p} \tag{34}$$

and for the case of the plane channel flow they are shown on Fig. (4b).

The problem with continuous definition of the boundary condition for ε is similar to $\mathcal{P}$, so the blending according to Eq. (32) is straightforward. Only the coefficient in the exponent of the blending function was modified due to specific and strong variation of ε in the near-wall region:

$$\varepsilon_p = \frac{2\nu k_p}{y_p^2} e^{-\Gamma_\varepsilon} + \frac{c_\mu^{3/4} k_p^{3/2}}{\kappa y_p} e^{-1/\Gamma_\varepsilon} \tag{35}$$

where $\Gamma_\varepsilon = 0.001 y^{+4}/(1+y^+)$.

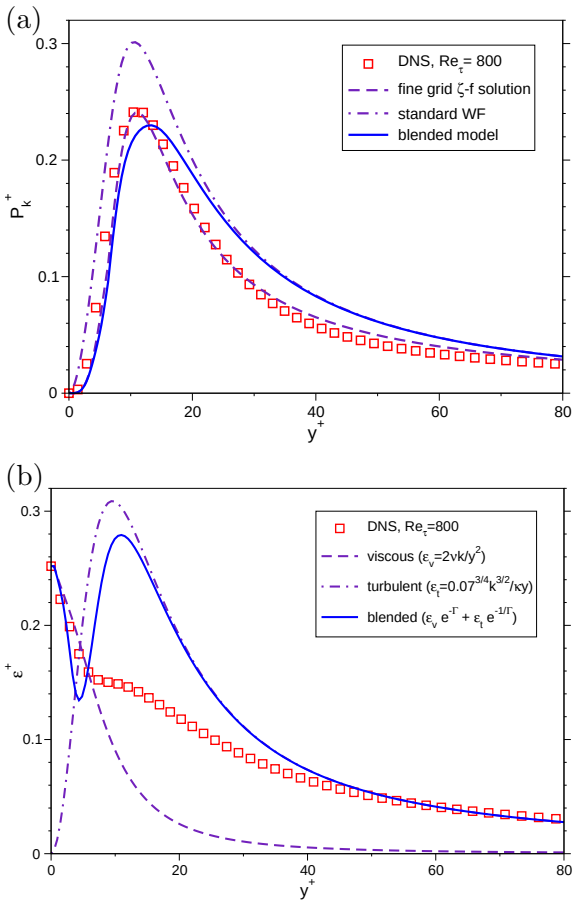

Figure 4: The fine mesh (integration to the wall – dashed line) and the coarse mesh (wall function approach – dash-dotted line) solution of the production $\mathcal{P}$ (a), and the dissipation ε (b) in the plane channel flow [5]. Full line: adopted blending model (Eq. 33 and Eq. 35). Symbols: DNS of Tanahashi *et al.* [5].

It is noted, however, that for the turbulent region ε_t is tied to $\mathcal{P}_t$: Fig. (5) shows that the production and the dissipation rate, as well as their averaged values are nearly equal in the fully turbulent region. Therefore even the simpler model, like Eq. (26), performs reasonably well as a near-wall treatment.

4.3 Elliptic relaxation function

For this function, none of the blending formulations (25), (26) or (32) is adequate for the CWT, for two reasons. First, the wall-limit ("viscous") value of f ($f_v = -2\nu\zeta_p/y_p^2$) and its homogeneous value ($f_h = (C_1 - 1 + C_2'\mathcal{P}/\varepsilon)(\zeta - 2/3)/\tau$) have opposite signs. Second, while f_v ranges from its wall (negative) value to zero, f_h ranges from (positive) infin-

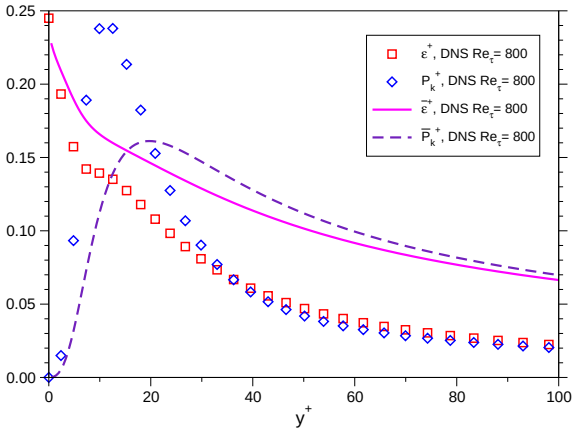

Figure 5: Distribution of ε and $\mathcal{P}$ and their averaged values in the channel flow. Symbols: DNS of Tanahashi *et al.* [5].

ity to its homogeneous value (tends to zero). Thus there is a huge difference between them in the buffer region, and no blending (except the full elliptic solution) can give a realistic solution there.

Therefore, the simplest wall treatment for f is to manage its boundary condition in the same way as for the standard ζ-f model with integration to the wall, i.e. to impose the wall value f_w obtained from the budget of Eq. (1):

$$f_w = \frac{-2\nu\zeta_p}{y_p^2} \tag{36}$$

This definition is correct if the near-wall cell lays in the viscous sublayer, and it gives zero value for f_w (it drops fast to zero, because of the power two in the denominator) away from the wall, which is incorrect. But since Eq. (36) sets only the boundary condition at the wall, the f equation (Eq. 10) will produce some approximate solution for the near-wall cell centre due to in-domain flow conditions. This is acceptable because the wall blocking effect (which f should describe) fades away in the far-field.

5 Test cases

As an illustration of performance of the proposed model and the near-wall treatment, we present the results of the computations of several test cases: a steady and pulsating plane channel flow, a round jet impinging into a flat plate and a flow separating on a backward facing step with heated bottom wall.

As a reference data for the channel flow calculation ($Re_\tau = 800$), the DNS results of Tanahashi *et al.* are taken. The ζ-f results, shown on Fig.(6), are obtained with very fine mesh (the first y^+ was the same like that used for DNS calculation), and the $\overline{v^2}$-f model could not give a convergent solution on that mesh.

(a)

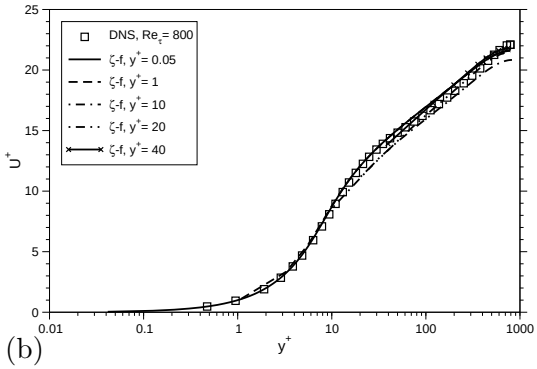

(b)

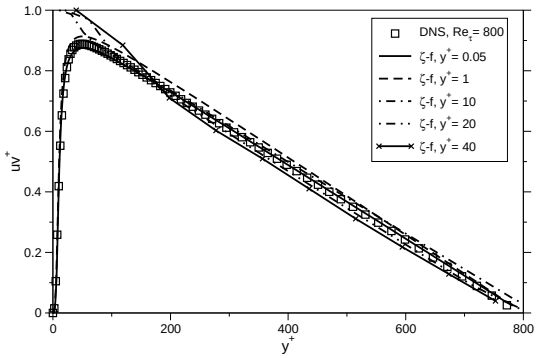

Figure 6: Profiles of velocity (a) and shear stress (b) for channel flow $Re_\tau = 800$. Symbols: DNS data of Tanahashi *et al.* [5]. Lines: ζ-f with CWT for different meshes, varying first y^+ from 0.05 to 40.

In order to test the performance of the wall function for the transient flows we calculated the pulsating turbulent channel flow with the Stokes length scale $l_S^+ = 14$, where $l_S^+ = \sqrt{2/\omega^+}$, $\omega^+ = \omega\nu/u_\tau$ and ω is the forcing frequency. For this case the near-wall treatment is also very important, because during the pulsating cycle the level of the turbulent kinetic energy is changing, varying thus the normalised distance from the wall of the near-wall cell centre. The reference data are LES results of Scotti and Piomelli [20], and the obtained results are given on Fig. (7).

It is clear from Fig. (7) that non-

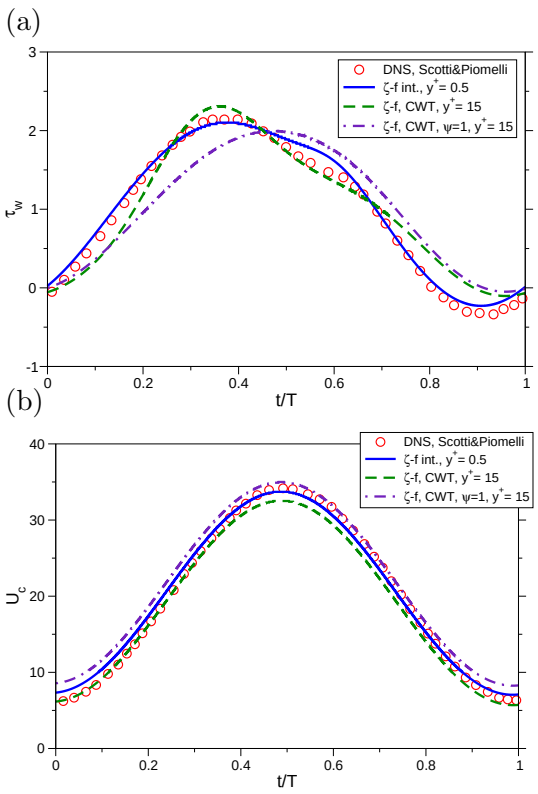

Figure 7: Results for the pulsating channel flow [20]: wall shear stress (a) and centerline velocity (b).

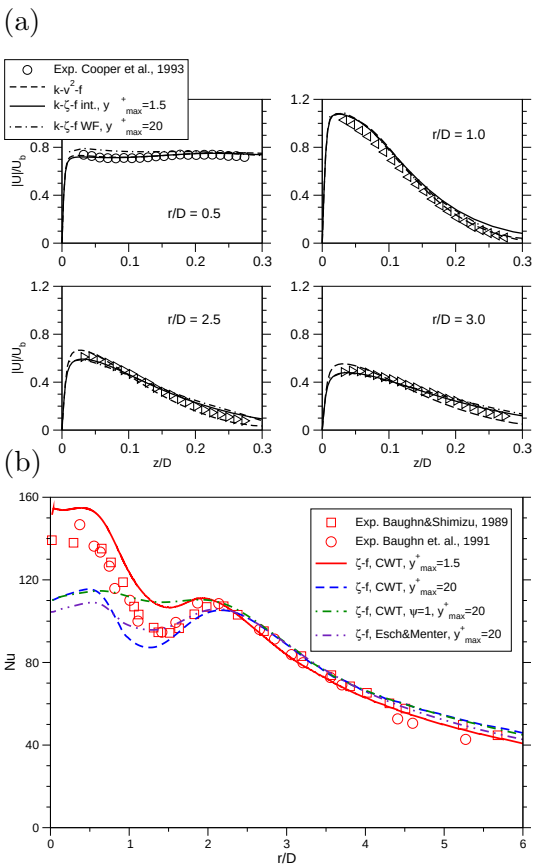

Figure 8: Velocity profiles at different distances from the jet centre (a) and Nusselt number distribution along the impingement plate (b) for $Re = 23000$. Symbols: experiments of Cooper *et al.* [9] for velocities; experiments of Baughn *et al.* [8] for Nusselt number. Dashed line: $\overline{v^2}$-f model with integration to the wall. Full line: ζ-f model with integration to the wall. Dash-dot-dash line: ζ-f model with wall function.

equilibrium correction factor ψ significantly improves the prediction. Putting $\psi = 1$, i.e. using standard wall function, negative wall shear stress cannot be reproduced. Additionally, there is a flat part of the profile close to τ_w maximum which standard wall function does not sense, whereas the wall function with the correstion factor does predict it, just like with integration to the wall.

The impinging jet flow was calculated for two Reynolds numbers: $Re = 23000$ for which the reference data are taken from the experiment of Boughn and Shimizu [7], and $Re = 70000$ for which the reference data are taken from the experiment of Yan [10] (see Fig. 8). Both test cases are for the aspect ratio $H/D = 2$, and both include the heat transfer calculation.

Similar to calculation of the channel flow, the mesh used to calculate impinging jet with ζ-f model was too fine in the wall-normal direction for the $\overline{v^2}$-f model. Therefore the adjustments on the ζ-f mesh were needed in order to obtain the convergent $\overline{v^2}$-f solution. The mesh used for CWT is the one used for standard k-$\overline{v^2}$ model with wall function. The overall quality of results for both models is good, and in agreement with the experiments. However, the ζ-f reproduces the dip in the Nusselt number distribution better then $\overline{v^2}$-f model (see Fig. 8).

The standard test case for separating flow, the backward facing step flow was computed with ζ-f model and CWT for Reynolds number $Re = 28000$. The results, shown on Fig. (10), are compared with the reference data, the experiments of Vogel and Eaton [6], and the results obtained with $\overline{v^2}$-f model.

Both models are giving satisfactory results, with $\overline{v^2}$-f model performing slightly better in the recovery region in comparison to ζ-f, as one can see from Fig. (10).

Another flow with separation was com-

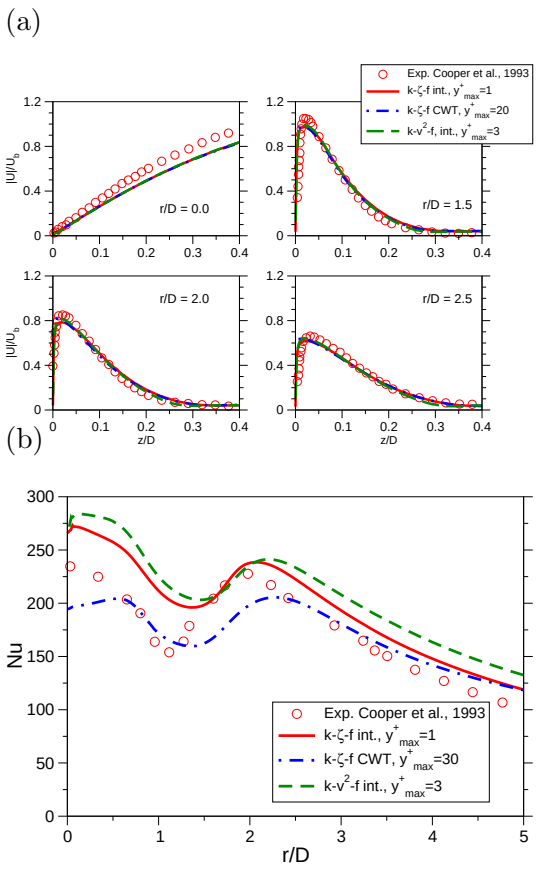

Figure 9: Velocity profiles at different distances from the jet centre (a) and Nusselt number distribution along the impingement plate (b) for $Re = 70000$. Symbols: experiments of Cooper *et al.* [9]. Dashed line: $\overline{v^2}$-f model with integration to the wall. Full line: ζ-f model with integration to the wall. Dash-dot-dash line: ζ-f model with wall function.

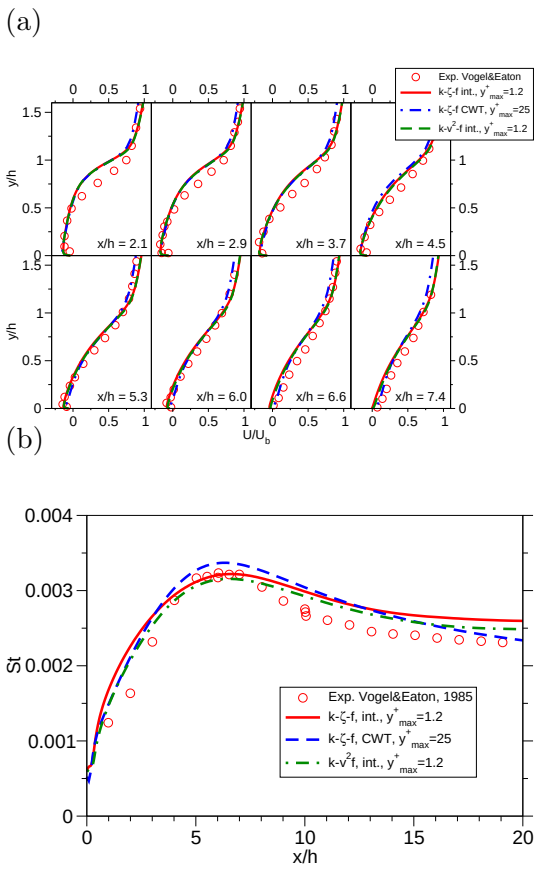

Figure 10: Velocity profiles at different distances behind a backward facing step (a) and Stanton number distribution along the heated wall (b). Symbols: experiments of Vogel and Eaton (1985). Full line: ζ-f model with integration to the wall. Dashed line: ζ-f model with CWT. Dashed-dot-dash line: $\overline{v^2}$-f model with integration to the wall.

puted both with $\overline{v^2}$-f and ζ-f model: the periodic flow over the smooth wavy wall (see Fig. 11). This case is challenging because the separation point is not defined by the geometry, unlike for the backward facing step where the fluid separates always at the step. Here the position of the separation point is defined by the local flow conditions, and in addition the occurrence of the reattachment and the separation are conjugated since the flow is periodic in the streamwise direction. Therefore the difficult part in this calculation is to get exact spearation and reattachment points. The reference data are obtained from the work of Temmerman and Lechziner [21], and the comparison of the results is shown on Fig. (11).

Acknowledgement

This work emerged from the *MinNOx* project sponsored by the Commission of the European Community, Contract ENK6-CT-2001-00530.

References

[1] Durbin P.A. Near-wall turbulence closure modelling without 'damping functions'. *Theoret. Comput. Fluid Dynamics*, **3**, 1991, pp. 1-13.

[2] Kader B.A. Temperature and concentration profiles in fully turbulent boundary layers. *Int. J. Heat Mass Transfer*, **24**, 1981, pp. 1541-1544.

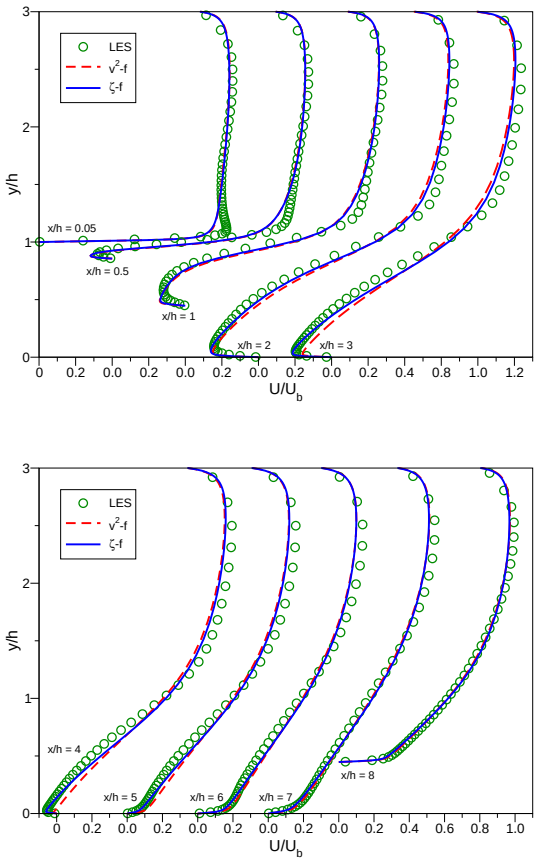

Figure 11: Profiles of U-component of the velocity at different distances in 2D wavy wall. Symbols: LES of Temmerman and Lechziner [21]. Full line: ζ-f model with integration to the wall. Dashed line: $\overline{v^2}$-f model with integration to the wall.

[3] Speziale, C.G., Sarkar, S. and Gatski, T. Modelling the pressure-strain correlation of turbulence: an invariant system dynamic approach. *J. Fluid. Mech.*, **227**, 1991, pp. 245-272.

[4] Esch, T. and Menter F.R. Heat Transfer Predictions Based on Two-Equation Turbulence Models with Advanced Wall Treatment. *Turbulence, Heat and Mass Transfer*, **4**, 2003, pp. 633-640.

[5] Tanahashi, M., Kang, S.-J., Miyamoto, S., Shiokawa, S. and Miyauchi, T. Scaling law of fine scale eddies in turbulent channel flows up to $Re_\tau = 800$. *Int. J. Heat Fluid Flow*, **25**, 2004, pp. 331-340.

[6] Vogel, J.C. and J.K. Eaton. Combined Heat Transfer and Fluid Dynamic Measurements Downstream of a Backward-Facing Step. *ASME, J. Heat Transfer*, **107**, 1985, pp. 922-929.

[7] Baughn, J. and Shimizu, S. Heat transfer measurements from a surface with uniform heat flux and an impinging jet. *ASME Journal of Heat Transfer*, **111**, 1989, pp. 1096-1098.

[8] Baughn, J.W., Hechanova, A.E. and Yan, X. An Experimental Study of Entrainment Effects on the Heat Transfer From a Flat Surface to a Heated Circular Impinging Jet. *Journal of Heat Transfer*, **113**, 1991, pp. 1023-1025.

[9] Cooper, D., Jackson, D.C., Launder, B.E. and Liao, G.X. Impinging jet studies for turbulence model assessment – I. Flow-field experiments. *Int. J. Heat Mass Transfer*, **36**, 1993, pp. 2675-2684.

[10] Yan, X. A preheated-wall transient method using liquid crystals for the measurement of heat transfer on external surfaces and in ducts. Ph.D. thesis, University of California, Davis, 1993.

[11] Hanjalic, K., Popovac, M. and Hadziabdic, M. A Robust near-wall elliptic-relaxation eddy-viscosity turbulence model for CFD. *Int. J. Heat Fluid Flow*, **25**, 2004, pp. 897-901.

[12] Craft, T.J., Gerasimov, A.V., Iacovides, H. and Launder, B.E. Progress in the generalisation of wall functions treatments. *Int. J. Heat Fluid Flow*, **23**, 2000, pp. 148-160.

[13] Durbin, P.A. On the k-ε stagnation point anomaly. *Int. J. Heat Fluid Flow*, **17**, 1996, pp. 89-90.

[14] Lien, F.S., Kalitzin, G. and Durbin, P.A. RANS modelling for compressible and transitional flows. *Proceedings of the Summer Program*, 1998, pp. 267-286.

[15] Laurence, D.R., Uribe, J.C. and Utyuzhnikov, S.V. A robust formulation of the v2-f model *Flow, Turbulence and Combustion*, 2004, in press.

[16] Behnia, M., Parniex, S. and Durbin, P.A. Prediction of heat transfer in an axisymmetric turbulent jet impinging on a flat plate. *Int. J. heat Mass Transfer*, **41**, 1998, pp. 1845-1855.

[17] Rotta, J. Statistiche Theorie nichhomogener Turbulenz, Part I. *Zeitschrift für Physik*, **129**, 1951, pp. 547-572.

[18] Popovac, M. and Hanjalic, K. Compound wall treatment for RANS computation of complex turbulent flow. *submitted to 3rd M.I.T. Conference, Boston, USA*, **xx**, 2004, pp. yyy-yyy.

[19] Nagano, Y., Tsuji, T. and Houra, T. Structure of turbulent boundary layer subjected to adverse pressure gradient. *Int. J. Heat Fluid Flow*, **19**, 1998, pp. 563-572.

[20] Scotti, A., and Piomelli, U. Numerical simulation of pulsating turbulent channel flow. *Phys. Fluids*, **13**, 2001, pp. 1367-1384.

[21] Temmerman, L. Large eddy simulation of separating flows from curved surfaces. Ph.D. thesis, Queen Mary University of London, London, U.K, 2004.

[22] Tummers, M.J., Hanjalic, K., Rodnik, R., Flikweert, M. and Moshfegh, B. Impinging jet cooling of wall mounted cubes. *submitted to ERCOFTAC Int. Symposium ETMM6, Sardinia, Italy*, **xx**, 2004, pp. yyy-yyy.